

Aliased Time-Modulated Array OFDM System

Marcin Wachowiak, *Member, IEEE*, André Bourdoux, *Senior Member, IEEE*, Sofie Pollin, *Member, IEEE*,

Abstract—The time-modulated array is a simple array architecture in which each antenna is connected to an RF switch that serves as a modulator. The phase shift is achieved by digitally controlling the relative delay between the periodic modulating sequences of the antennas. Two factors limit the practical use of this architecture. First, the switching frequency is high, as it must be a multiple of the sampling frequency. Second, the discrete modulating sequence introduces undesired harmonic replicas of the signal with non-negligible power. This paper exploits aliasing to simultaneously reduce sideband radiation and switching frequency. The transmit signal has a repeated block structure in the frequency domain to facilitate coherent combining of the aliased signal blocks. As a result, a factor A reduction in switching frequency is achieved at the cost of a factor A reduction in communication capacity. Doubling A reduces sideband radiation by around 2.9 dB. The feasibility of the proposed method is experimentally validated for wideband signals.

Index Terms—Time-modulated arrays (TMA), single-sideband time-modulated phased arrays (STMPA), phase modulation, beam steering, beamforming, sideband radiation

I. INTRODUCTION

A. Problem Statement

Antenna arrays are an essential component of current and future generations of wireless systems [1]. However, when considering conventional architectures, the scaling of antenna arrays raises concerns about cost, complexity, and energy efficiency [2], [3]. To address scaling problems, alternative array architectures should be considered [4]. A time-modulated array is a simple antenna array architecture in which each antenna is connected to the multi-throw switch that performs time modulation [5]. The idea was first proposed in [6]. To improve the efficiency of time modulation, the switch can be replaced with a low-resolution discrete phase shifter [7]. The simplicity of the switch, which is the primary building block of the front end, offers savings in cost, power, and size of the radio front end compared to mixers or high-resolution phase shifters [8], [9].

However, the simple architecture of TMA comes with a few limitations that prevent its widespread adoption. Firstly, in conventional time-modulated arrays, the switch must operate at a multiple of the sampling frequency to take advantage of oversampling to offer an improved phase-shifting resolution and prevent the overlap of the harmonics of the transmitted signal [5], [10], [11]. Secondly, due to the discretized modulating sequence, the time modulation introduces harmonic replicas of non-negligible power of the baseband signal at

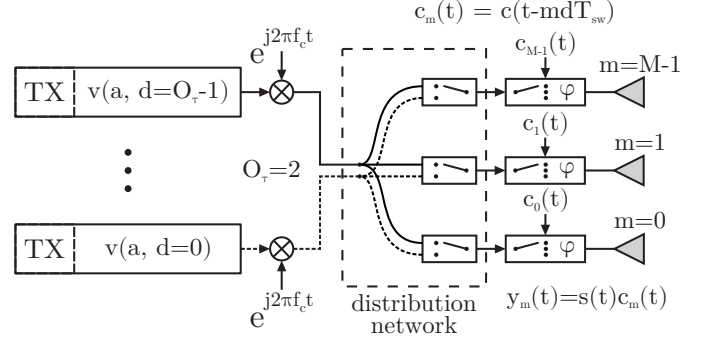


Fig. 1. Architecture of the aliased time-modulated transmit array. The baseband signal consists of A identical repeated blocks in the frequency domain. Each block is differently precoded by $v(a, d)$, depending on the block index a and selected delay value d . The oversampling factor O_r determines the number of required frequency precoders implemented as digital baseband units. Depending on the index d , each m -th antenna is fed by a selected precoder via a distribution network of standard RF switches.

multiples of the switching frequencies. [7], [12]. To comply with wireless standards, the sideband radiation (SR) must be suppressed, which requires an additional bandpass filter per antenna. To facilitate more widespread utilization of TMAs, methods are needed to reduce the switching frequency and suppress the sideband radiation. The harmonic components might be exploited to facilitate the simultaneous multi-beam operation with TMA [13], [14]. However, each harmonic beam transmits the same replicated baseband signal, limiting the practical application of transmit TMAs.

B. Relevant works

Initially, time-modulated arrays were analyzed under a narrowband scenario, considering just a single carrier. Various algorithms have been proposed to optimise the switching instants of the RF switches to minimise sideband radiation, including genetic [15], evolution [16], [17] and particle swarm [18] optimization algorithms. The modulating signal format determines the sideband radiation. To further reduce sideband radiation, the following approaches have been proposed: aperiodic modulating pulses [19], pseudorandom modulating sequence [20] or different switching frequency per element [21]. A significant improvement in the sideband suppression is observed when employing phase modulation [22], utilizing stepped waveforms [23] or simultaneous amplitude and phase modulation (IQ) [24]–[26]. The interest in the TMA architecture has resulted in practical implementations which utilize simple low-bit switched delay lines as building blocks [27], [28].

The listed approaches are suitable for narrowband signals, and the switching frequency is assumed to be much higher than the transmitted signal bandwidth. This leads to an assumption

Marcin Wachowiak and Sofie Pollin are with Interuniversitair Micro Electronica Centrum, 3001 Leuven, Belgium and also with the Katholieke Universiteit Leuven, 3000 Leuven, Belgium (e-mail: marcin.wachowiak@imec.be)

André Bourdoux is with Interuniversitair Micro-Electronica Centrum, 3001 Leuven, Belgium. (Corresponding author: Marcin Wachowiak)

TABLE I
STATE-OF-THE-ART COMPARISON

Reference	Modulation	Max measured SR [dB]	f_{sw}	Optimization required
[19]	Binary amplitude	-35.98	$\gg B$	No
[21]	Binary amplitude	-36.94	$\gg B$	Yes
[20]	Phase and binary amplitude	-39.4	$\gg B$	No
[24]	IQ	-33.3	$\gg B$	Yes
[25]	IQ	-33.57	$\gg B$	Yes
[29]	IQ	-13.98	$\gg B$	No
[26]	IQ	-16.9	$\gg B$	No
This work	Phase	-6.57 ¹	$\ll B$	No

of an arbitrary and unconstrained timing resolution of a switch. For wideband signals, this assumption is no longer valid and the switching frequency becomes constrained by signal bandwidth and quickly approaches limits imposed by hardware. Moreover, the extent of the sideband radiation is increased as the baseband signal now has a greater width in the frequency domain, increasing the strain on filtering requirements.

C. Contributions

This work considers the TMA combined with a wideband OFDM signal and proposes a method to simultaneously reduce the switching frequency and the sideband radiation by introducing aliasing between the harmonic replicas of the transmitted signal. It is achieved at the cost of the effective bandwidth as the baseband signal, in the frequency domain, is composed of A repeated blocks, which are differently pre-coded. The improvement in sideband suppression and spectral efficiency trade-off is discussed in detail. The oversampling of the modulating sequence for improved resolution beamforming with aliased TMA is proposed and studied. The feasibility of the proposed method is validated experimentally for wideband signals.

Table I presents the work with reference to the state-of-the-art. Note that binary amplitude modulation has low efficiency due to the switching off of the transmitted signal. The IQ modulation requires complex hardware and to achieve low SR values, optimization is required, which is cumbersome in real-time applications. All of the reported works require a switching frequency higher than the signal bandwidth. The proposed solution offers a low complexity and scalable method to simultaneously reduce sideband radiation and switching frequency. In the proposed method, the maximum measured SR is primarily determined by the phase shifter resolution. The aliasing still improves the maximum SR compared to a system without it; however, its primary benefit is the reduction of the sideband radiation over a wide bandwidth. When

¹Based on the minimal working example with $N = 2$ and $A = 128$. The maximum measured SR is reduced to -18.66 dB if 1% transition bandwidth is considered and -36.32 dB for 10%. See the experimental results in Sec. III.

some transition bandwidth is considered, the maximum SR is significantly reduced due to the steep spectral roll-off of the aliased OFDM spectra.

II. SIGNAL MODEL

A. Time modulation

Consider a time-modulated antenna, which is connected to the N -throw/state switch. The RF switch acts as a discrete phase shifter - each state of the switch results in a different phase shift of the input signal. The phase shift of the n -th switch state is given by

$$\varphi(n) = 2\pi \frac{n}{N}, \quad (1)$$

where n is the index of the state $n \in \{0, 1, \dots, N-1\}$. The switch operates at the sampling frequency f_s corresponding to a signal of bandwidth B . The pulse duration of each state is

$$T_p = AT_s, \quad A \in \mathbb{N}^+, \quad (2)$$

where A is the aliasing factor that increases the pulse duration and reduces pulse frequency and $T_s = 1/f_s$. The pulse frequency is

$$f_p = \frac{1}{T_p} = \frac{f_s}{A}. \quad (3)$$

The modulating signal is a periodically repeated sequence of N rectangular pulses with a phase given by (1), for the case of linear phase steps, which results in maximization of the power at the first harmonic [7]. Due to the discretized switching instants and phase shift values, the basic building block of the TMA modulating signal is a rectangular pulse. Consider a periodic rectangular pulse of duration T_p with unit amplitude and phase shift of $\varphi(n)$. The time domain representation of the pulse is given by

$$g_n(t) = e^{j\varphi(n)} \sum_{i=-\infty}^{\infty} \text{rect}\left(\frac{t}{T_p} - \frac{T_p}{2} + iNT_p\right). \quad (4)$$

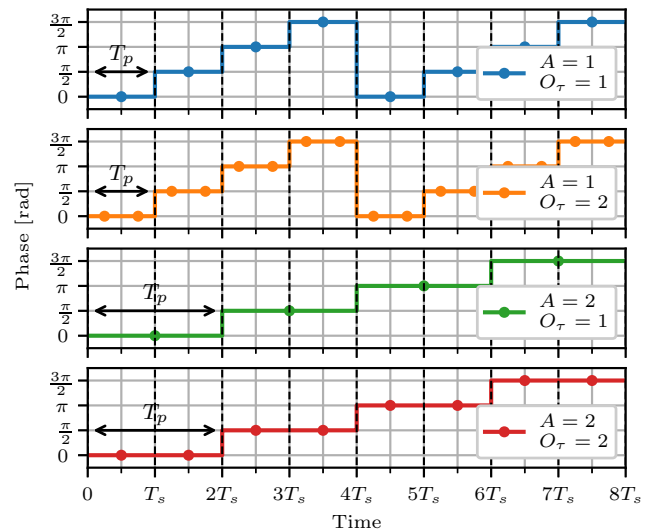


Fig. 2. Modulating signal of the ATMA for $N = 4$ and different aliasing A and oversampling O_τ factors.

Fig. 2 illustrates the modulating signal in the time domain.

The pulse is periodic with a period NT_p , which allows expanding it into a Fourier series. The Fourier coefficient of the k -th harmonic component is given by

$$G_n(k) = e^{j\varphi(n)} \text{sinc}\left(\pi \frac{k}{N}\right) e^{-j\pi \frac{k}{N}}, \quad (5)$$

where $\text{sinc}(x) = \sin x/x$. The modulating (control) signal $c(t)$ is composed of a sequence of N delayed complex pulses from (4) resulting in

$$c(t) = \sum_{n=0}^{N-1} g_n(t - nT_p). \quad (6)$$

The frequency domain representation of the modulating signal is

$$\begin{aligned} C(k) &= \frac{1}{N} \sum_{n=0}^{N-1} G_n(k) e^{-j2\pi \frac{n}{N} T_p f_p} \\ &= \text{sinc}\left(\pi \frac{k}{N}\right) e^{-j\pi \frac{k}{N}} I(k) \end{aligned} \quad (7)$$

$I(k) = \frac{1}{N} \sum_{n=0}^{N-1} e^{j2\pi \frac{n}{N} (1-i)}$ determines the existence of the i -th spectral component at frequency $f_k = \frac{i}{N} f_p$

$$I(k) = \begin{cases} 1, & k = 1 + zN \\ 0, & k \neq 1 + zN \end{cases}, \quad z \in \mathbb{Z} \quad (8)$$

To simplify the following analysis, the discrete harmonic representation of the modulating sequence is transformed into a continuous frequency range

$$C(f) = \alpha(i) \delta\left(f - \left(\frac{f_p}{N} + if_p\right)\right) \quad (9)$$

where $\alpha(i) = \text{sinc}\left(\pi\left(i + \frac{1}{N}\right)\right) e^{-j\pi\left(i + \frac{1}{N}\right)}$ is the complex coefficient determining the amplitude and phase of the i -th harmonic component and δ is the Dirac delta function. The i -th harmonic components are located at frequency $\frac{f_p}{N} + if_p$. To gain more insight into the amplitude and phase of the harmonic components, $\alpha(i)$ can be expressed as

$$\alpha(i) = \left| \text{sinc}\left(\pi\left(i + \frac{1}{N}\right)\right) \right| e^{j\phi_{\alpha}(i)}, \quad (10)$$

where ϕ is the function describing the phase of the $\alpha(i)$ harmonic component

$$\phi_{\alpha}(i) = \begin{cases} -\frac{\pi}{N}, & i \geq 0 \\ -\frac{\pi}{N} - \pi, & i < 0 \end{cases}. \quad (11)$$

The length of the modulating sequence N affects the power of the harmonics by narrowing the main lobe of the sinc function. The frequency shift of the total signal is equal to $f_{\text{mod}} = f_p/(NA)$ - the modulating frequency. The length N affects the phase of the harmonic components; however, note that the relative difference between the positive and negative components is constant and equal to π . The aliasing factor A reduces the spacing of harmonic components and the total frequency shift of the transmitted signal. Fig. 3 shows the power and phase of the harmonics for $A = 1$ and selected values of N .

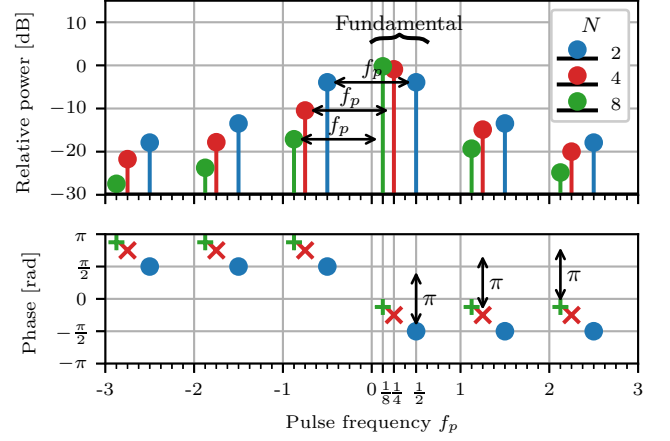


Fig. 3. Power and phase of the harmonic components of the time modulating signal for $A = 1$ and selected values of N .

B. Phase shifting

The phase shifting of the signal is achieved by a cyclic shift of the modulating sequence. Consider an oversampling factor O_τ that increases the operating frequency of the switch O_τ times. The pulse duration is unaffected as the previous phase states are repeated to keep it constant, see Fig. 2. The switching frequency that has to be supported by the switch is

$$f_{\text{sw}} = f_s \frac{O_\tau}{A}. \quad (12)$$

Note that in order to have a switching frequency lower than the signal bandwidth, the oversampling factor should always be lower than the aliasing factor, $O_\tau \leq A$. The oversampling allows for obtaining a refined timing resolution, which results in a multiplied number of effective phase shifts. Given a sequence of length N and pulse duration T_p , there are D possible discrete delay values given by

$$D = N \frac{T_p}{T_{\text{sw}}} = N \frac{T_p}{\frac{T_p}{O_\tau}} = NO_\tau, \quad (13)$$

where $T_{\text{sw}} = 1/f_{\text{sw}}$. An example of an oversampled modulating signal is shown in Fig. 2. The delay (cyclic shift) of the time domain modulating sequence is equivalent to the phase rotation in the frequency domain as follows

$$\begin{aligned} C(f, d) &= \mathcal{F}\{c(t - dT_{\text{sw}})\} \\ &= \alpha(i) e^{-j2\pi d T_{\text{sw}} f} \delta\left(f - \frac{f_p}{N} - if_p\right), \end{aligned} \quad (14)$$

where $d \in \{0, 1, \dots, D-1\}$ is the index of the selected digital delay. The phase shift due to the cyclic delay of the phase modulating sequence is

$$\begin{aligned} \varphi_\tau(i, d) &= -2\pi d T_{\text{sw}} \left(\frac{f_p}{N} + if_p\right) \\ &= -2\pi \frac{d}{D} - 2\pi \frac{d}{O_\tau} i. \end{aligned} \quad (15)$$

It can be seen that the oversampling increases the phase-shifting resolution by an order of O_τ . However, for d values

other than multiples of O_τ , there is an additional phase shift dependent on the harmonic index i . Extending (10) with (15) to include the effects of the time delay on the harmonic component results in

$$\alpha(i, d) = \alpha(i) e^{j\varphi_\tau(i, d)}. \quad (16)$$

C. Aliasing

The maximum bandwidth of the signal transmitted by the conventional TMA to avoid aliasing is determined by the spacing of the harmonic components equal to f_s/A (3). In this paper, aliasing combined with the block structure of the signal in the frequency domain and precoding is exploited to introduce destructive interference between the harmonics of the transmitted signal to reduce the sideband radiation. Consider a baseband signal of bandwidth $B = f_s$ that consists of A (aliasing factor) joint/adjacent rectangular blocks of equal width B/A in the frequency domain. The frequency domain representation of the single block is

$$S_a(f) = v(a) \text{rect} \left(\frac{f}{\frac{f_s}{A}} \right), \quad (17)$$

where $v(a)$ is complex frequency-flat precoding coefficient per block and $a \in \{0, 1, \dots, A-1\}$ is the block index. The total baseband signal can be written as a convolution of a precoded finite Dirac delta comb of length A and a rectangular function

$$\begin{aligned} S(f) &= \sum_{a=0}^{A-1} S_a \left(f - a \frac{f_s}{A} + \frac{A-1}{2A} f_s \right) \\ &= \text{rect} \left(\frac{f}{\frac{f_s}{A}} \right) * \sum_{a=0}^{A-1} v(a) \delta \left(f - \left(a - \frac{A-1}{2} \right) \frac{f_s}{A} \right). \end{aligned} \quad (18)$$

The time modulation of this signal with a precoded-shifted frequency-domain representation is achieved by multiplying the time domain signal with a modulating sequence $C(f, d)$, which in the frequency domain corresponds to the convolution of (9) with (18)

$$\begin{aligned} Y(f, d) &= S(f) * C(f, d) \\ &= \sum_{a=0}^{A-1} v(a) \alpha(i, d) \delta \left(f - \left(a - \left\lfloor \frac{A-1}{2} \right\rfloor + \Delta_f + i \right) \frac{f_s}{A} \right) \\ &\quad * \text{rect} \left(\frac{f}{\frac{f_s}{A}} \right), \end{aligned} \quad (19)$$

where $\Delta_f = \left\lfloor \frac{A-1}{2} \right\rfloor - \frac{A-1}{2} + \frac{1}{N}$ is a fractional shift in frequency due to time modulation and centering of the convolution kernel $v(a)$. The aliased signal with overlapping frequency blocks can be written as

$$\begin{aligned} Y(f, d) &= \sum_{a=0}^{A-1} v(a) \alpha \left(i - a + \left\lfloor \frac{A-1}{2} \right\rfloor, d \right) \\ &\quad \text{rect} \left(\frac{f}{\frac{f_s}{A}} \right) * \delta \left(f - (\Delta_f + i) \frac{f_s}{A} \right) \\ &= \alpha_A(i, d) \text{rect} \left(\frac{f}{\frac{f_s}{A}} - (\Delta_f + i) \right). \end{aligned} \quad (20)$$

where $\alpha_A(i, d)$ is the complex coefficient resulting from aliasing of A precoded harmonic components $\alpha(i, d)$. Expanding $\alpha(i, d)$ with (16) and (15) gives

$$\begin{aligned} \alpha_A(i, d) &= e^{-j2\pi \frac{d}{B}} e^{-j2\pi \frac{d}{O_\tau} i} e^{-j2\pi \frac{d}{O_\tau} \left\lfloor \frac{A-1}{2} \right\rfloor} \\ &\quad \sum_{a=0}^{A-1} v(a) e^{j2\pi \frac{d}{O_\tau} a} \alpha \left(i - a + \left\lfloor \frac{A-1}{2} \right\rfloor \right) \end{aligned} \quad (21)$$

D. Precoder design

The destructive interference of the sideband radiation is achieved by the design of the precoding vector $v(a)$. However, oversampling introduces an additional phase component $e^{j2\pi \frac{d}{O_\tau} a}$ in the sum of (21). To compensate for the phase shift, the precoder is extended with a conjugate of it

$$v(a, d) = v(a) e^{-j2\pi a \frac{d}{O_\tau}}. \quad (22)$$

The oversampling O_τ determines the periodicity of the phase shift and the number of additional precoding vectors required to compensate for it across all d values. The precoder is chosen based on the d value per antenna. When considering oversampling, multiple precoders are required, increasing the complexity of the array architecture. As digital precoding is required, the precoders are implemented as separate digital basebands. The number of digital baseband units does not scale with antennas. However, each antenna might require a different precoder, which can be provided by a switched distribution network, as shown in Fig. 1. Given the extended precoder the sum in (21) simplifies to

$$\alpha_A(i, d) = e^{j\varphi_{\tau A}(i, d)} \sum_{a=0}^{A-1} v(a) \alpha \left(i - a + \left\lfloor \frac{A-1}{2} \right\rfloor \right), \quad (23)$$

where $e^{j\varphi_{\tau A}} = e^{-j2\pi \frac{d}{B}} e^{-j2\pi \frac{d}{O_\tau} (i + \left\lfloor \frac{A-1}{2} \right\rfloor)}$ is the phase shift due to the selected delay value d . The desired baseband signal is within the harmonic indices $i_{\text{bb}} \in \{-(A-1) + \left\lfloor \frac{A-1}{2} \right\rfloor, \dots, \left\lfloor \frac{A-1}{2} \right\rfloor\}$. All other harmonic components $i \notin i_{\text{bb}}$ are considered sideband radiation and should be minimized. By evaluating the phase of the harmonic components for $i > \left\lfloor \frac{A-1}{2} \right\rfloor$ it can be seen that the argument of α in (23) is always positive, resulting in constant phase given by (11) for all positive sideband harmonic indices. Similarly for the negative sideband indices $i < -(A-1) + \left\lfloor \frac{A-1}{2} \right\rfloor$ the argument of α is always negative. Therefore, the harmonics on the positive and negative sides of the sideband have a constant phase within each sideband. The amplitude of the harmonic components decreases with increasing $|i|$. Each sideband exhibits a different monotonicity and rate of change/slope (for $N > 2$) of the amplitude of the harmonic components. This renders the amplitude precoding cumbersome and limits its feasibility.

In the following, a phase-only precoder is considered to minimize both sidebands simultaneously. Given the constant phase of the summed sideband harmonic components, a natural choice to minimize the sum is to alter the sign of the summed components by applying an alternating precoder

$$v(a) = (-1)^a = e^{j\pi a}. \quad (24)$$

The alternating precoder introduces destructive interference between the harmonic components at the sidebands at the cost of introducing power variations in the power of the passband signal. The fluctuations result from the summation of a different subset of precoded harmonic components. The 0-th harmonic component dominates the amplitude of the result and determines the phase. Note, that the aliased signal in the desired passband range has an alternating phase precoding, which can be easily compensated at the receiver. After the convolution/aliasing, indices of baseband signal of interest have a flipped range $i_{bbA} = \{-\lfloor \frac{A-1}{2} \rfloor, \dots, A-1 - \lfloor \frac{A-1}{2} \rfloor\}$.

Fig. 4 illustrates the signal processing steps in the aliased TMA system with $A = 2$ blocks. Fig. 4a presents the precoded baseband signal (18) in the frequency domain. Fig. 4b shows the harmonic components of the modulating signal from (10) with the color denoting the phase of each harmonic component. Next, the precoded baseband signal is multiplied

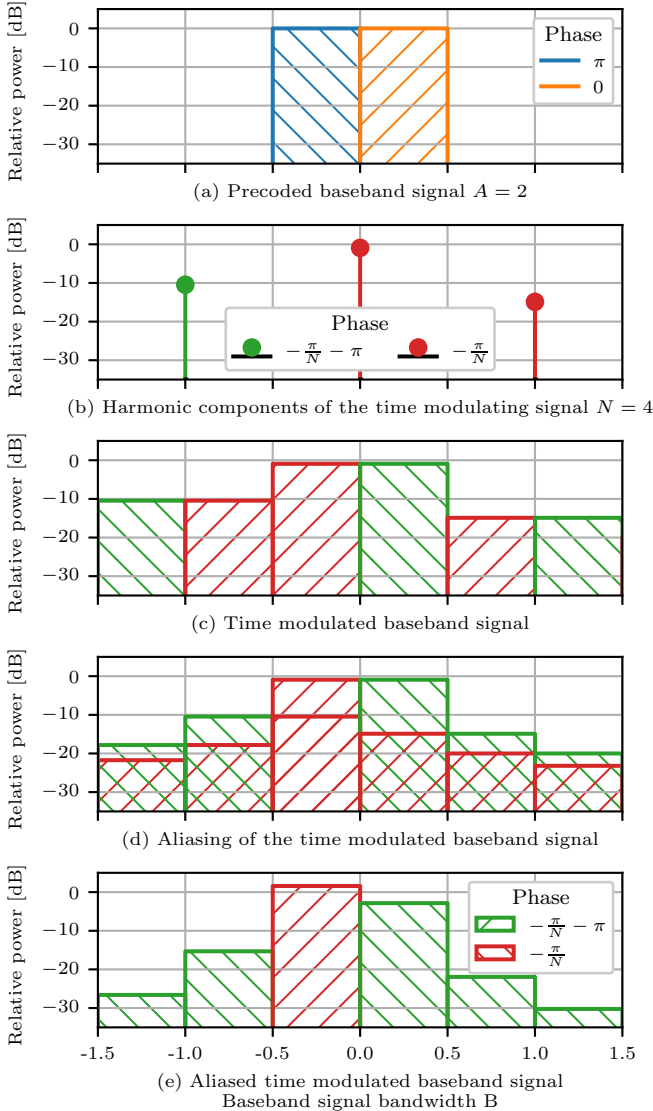


Fig. 4. Illustration of the aliasing for $N = 4$ and $A = 2$, no oversampling $O_\tau = 1$.

by the modulating signal, which corresponds to convolution in the frequency domain, resulting in replication of the baseband spectrum with altered phase precoding as shown in Fig. 4c. Note how the precoder phase affects the resultant phase of the blocks after the time modulation. To emphasize the phases of the baseband blocks, before aliasing and hence the spacing of the harmonics, the modulating frequency is set to be equal to the baseband bandwidth B in Fig. 4b and 4c. The aliasing of the differently precoded baseband blocks is illustrated in Fig. 4d according to (20). The aliasing in Fig. 4d and 4e is achieved by reducing the modulating frequency by 2, making it $B/2$. At the same time, the baseband bandwidth stays the same, resulting in an overlap of neighbouring blocks. Fig. 4d shows the phases of the aliased blocks before combining. It helps to observe where the noncoherent combination occurs and estimate the resulting power per block. Finally, Fig. 4e shows the sum of the aliased baseband blocks from Fig. 4d with visible attenuation of the sideband blocks. Note that the phase after the aliasing is not uniform across baseband blocks, which has to be taken into account at the receiver.

Fig. 5 shows the signal power spectrum at the time-modulator output for $N = 4$ and selected values of the aliasing factor A . The aliasing with an alternating precoder effectively reduces the power of the sideband radiation while introducing slight variations (ripple) in the power of the transmitted signal in the center of the spectrum. The sideband radiation cancellation is less effective for an odd A - an odd number of aliasing terms due to a lack of balance in the number of summed positively and negatively precoded components. Due to the poorer performance of the aliased system with odd values of A , the remaining results consider only even values of A .

The peak-to-peak power variations per block are determined mainly by N , and increasing A has a limited impact as the amplitude difference of the adjacent harmonics determines the summation result. Increasing N improves the power of the main harmonic while reducing the power of other, reducing the ripple. Fig. 6 presents the maximum power difference between the blocks in the frequency domain within the band of interest

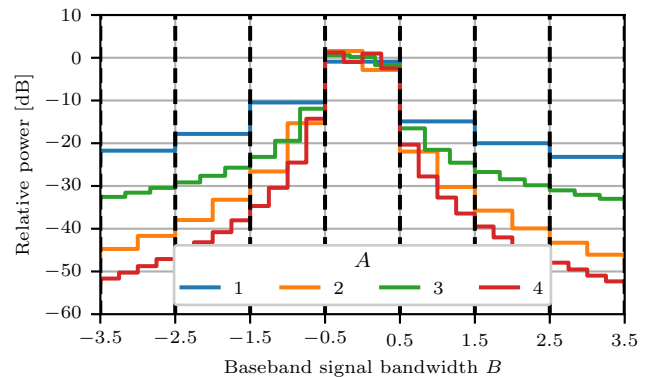


Fig. 5. Spectrum of TMA with considered block signal in frequency domain for $N = 4$ and selected values of A . (The frequency shift due to modulation is neglected.)

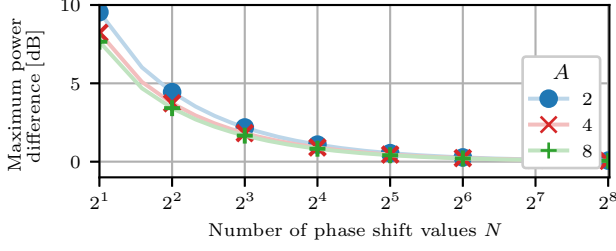


Fig. 6. The maximum power difference between blocks in the passband due to aliasing for selected values of A .

as a function of N . The power variations become negligible for $N \geq 16$.

The proposed system offers two ways of reducing the sideband power. The first is by increasing the number of switch states and phase shifts N , which narrows the sinc lobe, see (5). The second is by increasing the aliasing factor A . To quantify the reduction in the sideband power, the adjacent channel leakage ratio (ACLR) is used as a figure of merit. The ACLR is defined as

$$\text{ACLR} = \frac{\sum_{i \in i_{\text{bbA}}} |\alpha_A(i)|^2}{\sum_{i \in (i_{\text{bbA}} - A)} |\alpha_A(i)|^2}. \quad (25)$$

Fig. 7 presents the ACLR for a fixed number of blocks A for a varying number of phase shifts N . The dashed black line denotes the 5G minimum requirement of 45dB [30]. The introduction of aliasing improves the ACLR by around 7 dB compared to a system without it. Each doubling of N improves the ACLR by around 6.1 dB at the cost of increased hardware complexity. Fig. 8 shows the ACLR for fixed values of N

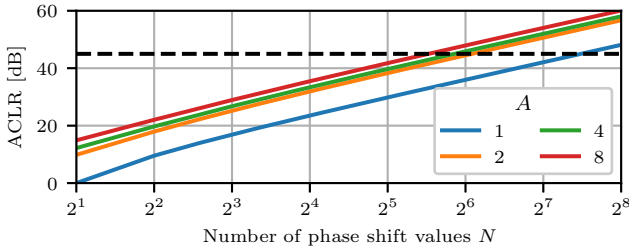


Fig. 7. ACLR versus the number of phase shift values N for selected number of blocks A .

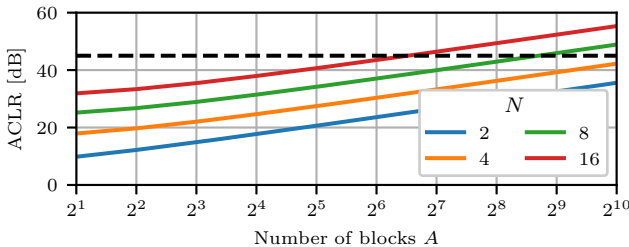


Fig. 8. ACLR versus the number of blocks A for selected number of phase shift values N .

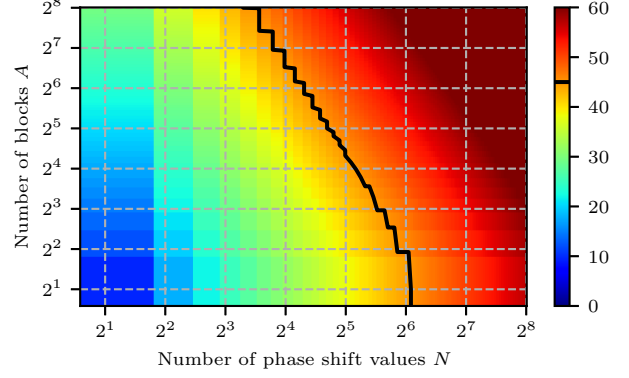


Fig. 9. TMA ACLR as a function of number of blocks A and the number of the phase shifter steps N . The black line denotes the 5G minimum requirement of 45 dB [30].

and a varying number of blocks A . For a small number of blocks, the ACLR gains are minor; however, as A increases, each doubling of A improves the ACLR by around 2.9 dB. Aliasing reduces the power of the sideband radiation without extensive hardware modifications. As shown by Fig. 7 and 8, satisfying the minimum ACLR for small values A or N requires the other parameter to be significantly large, which is not feasible. To meet the requirements, a reasonable approach is to optimize both parameters simultaneously. Fig. 9 presents the ACLR as a function of N and A . The black line denotes the 5G requirement of a minimum of 45 dB [30]. By tuning both parameters, an acceptable ACLR performance is reached for N and A equal to 2^5 instead of requiring $N = 2^7$ when $A = 2$.

E. Beamforming with aliased TMA

The ULA TMA array is considered to be operating in the far field with isotropic antenna elements spaced by d_λ . Taking the first element as a reference, the path difference per antenna element in the direction θ is

$$\Delta d_m = m d_\lambda \frac{c}{f_c} \sin(\theta), \quad (26)$$

where d_λ is the spacing between antenna elements expressed in wavelengths and f_c is the center frequency. To achieve beamforming, the modulating signal per antenna is cyclically shifted by md samples. The phase shift at the m -th antenna according to (23) is then

$$\phi_m(i, d) = -2\pi m \frac{d}{D} \left(1 + \left(i + \left\lfloor \frac{A-1}{2} \right\rfloor \right) N \right). \quad (27)$$

The array factor (AF) of the TMA at the i -th harmonic frequency for a selected delay d is

$$AF(\theta, i, d) = \alpha(i) \frac{1}{\sqrt{M}} \sum_{m=0}^{M-1} e^{j\phi_m(i, d)} e^{-j2\pi \frac{\Delta d_m}{c}} \left(f_c + \frac{f_p}{N} + i f_p \right). \quad (28)$$

where the factor $1/\sqrt{M}$ normalizes the total transmitted power to unity. Assuming that the frequencies of the harmonic

components with significant power are negligible compared to the carrier frequency $(\frac{1}{N} + i) f_p \ll f_c$ the AF can be simplified to

$$AF(\theta, i, d) = \alpha(i) \frac{1}{\sqrt{M}} \sum_{m=0}^{M-1} e^{-2\pi m d (\frac{1}{D} + \frac{1}{O_\tau} (i + \lfloor \frac{A-1}{2} \rfloor)) + d_\lambda \sin(\theta)} \quad (29)$$

Depending on the harmonic index and delay value, the formed beams are pointed in directions

$$\theta(i, d) = -\arcsin \left(\frac{d}{d_\lambda} \left(\frac{1}{D} + \frac{1}{O_\tau} \left(i + \left\lfloor \frac{A-1}{2} \right\rfloor \right) \right) \right). \quad (30)$$

In the presence of oversampling $O_\tau \geq 2$, the beamforming directions depend on the harmonic index i . When d is not a multiple of O_τ , the phase shift across the passband blocks $i \in i_{bb_A}$ is not the same, leading to different beamforming directions depending on the block index. As a result, only $A \frac{d}{O_\tau}$ blocks are beamformed in the desired direction, reducing the effective bandwidth, while the remaining harmonics are beamformed in other directions. Fig. 10 shows the phase shift per harmonic index and the effect of varying phases across blocks when oversampling is considered.

The oversampling effectively improves the phase shifting resolution, and given the reduced switching frequency, it can be easily achieved. However, its feasibility is limited due to the loss of effective beamformed bandwidth and the requirement of an additional precoding vector and signal distribution for each oversampling factor.

F. System considerations

When designing an ATMA system, the choice of the parameters A , N , O_τ is constrained. The phase shift of the block with index $a = i_{bb} + \lfloor \frac{A-1}{2} \rfloor$ due to delay is given by

$$\begin{aligned} \Delta\phi(a) &= \arg(\alpha_A(i_{bb}, d+1)) - \arg(\alpha_A(i_{bb}, d)) \\ &= -2\pi \frac{1}{O_\tau} \left(\frac{1+aN}{N} \right) \end{aligned} \quad (31)$$

To guarantee that each a block (within i_{bb}) observes the same relative phase shift, the following constraints arise

$$1 + aN \neq pO_\tau, \quad p \in \mathbb{N}^+ \quad (32)$$

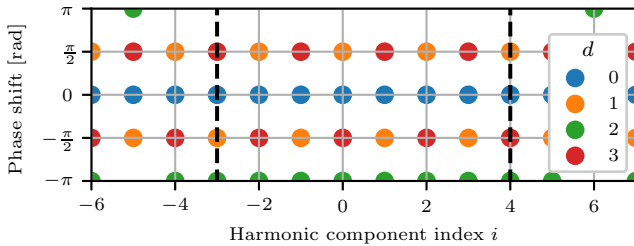


Fig. 10. Phase shift of harmonic components for different values of d normalized with regard to $d = 0$. For $A = 8$, blocks, $N = 2$, and $O_\tau = 2$. The black dashed lines denote the range of the desired baseband indices $i \in i_{bb_A}$.

and

$$\gcd(1 + aN, O_\tau) = 1. \quad (33)$$

The $1 + aN$ and O_τ must not have a common divisor for all considered a . The constraints are satisfied for all a if both O_τ and N are even; otherwise, limitations regarding A occur. Moreover, the number of samples corresponding to the modulation symbol duration must be a multiple of the modulating sequence length N . So that at least one complete cycle of time modulation occurs within the symbol duration. This requires upsampling of the modulation symbol at least by a factor N , which, for a single carrier system, further reduces the system's capacity. Due to the required extended duration of the modulation symbols in the time domain and the block structure of the transmitted signal, Orthogonal Frequency Division Multiplexing (OFDM) modulation is a natural choice for ATMA.

Consider an OFDM modulator with $K = AK_b$ subcarriers, where K_b is the number of subcarriers per block. To satisfy the constraint that the integer number of time modulation cycles should happen within a single symbol duration, the number of subcarriers per block must be a multiple of the number of phase shift steps

$$K_b = pN, \quad p \in \mathbb{N}^+ \quad (34)$$

The same applies to the length of a cyclic prefix if considered. The general preference for choosing K and N as a power of 2 requires O_τ and A also to be a power of 2. The repeated block structure of the signal in the frequency domain reduces the communications capacity of the system as the aliasing factor A increases. Due to aliasing, the symbol rate of the system of B bandwidth is

$$R = \frac{B}{A} \frac{K}{K + N_{cp}}, \quad (35)$$

where N_{cp} is the cyclic prefix length. The repeated modulation symbols in the frequency domain offer improved outage probability, but combining them does not improve SNR due to increased noise bandwidth. The power fluctuations per block in the passband might result in different SNRs being received at each block, resulting in SNR and capacity loss. Note that repetition in the frequency domain increases the peak-to-average power ratio. In the presence of a nonlinear amplifier, the signal is more susceptible to distortion. Fig. 11 presents the normalized capacity of the aliased TMA system.

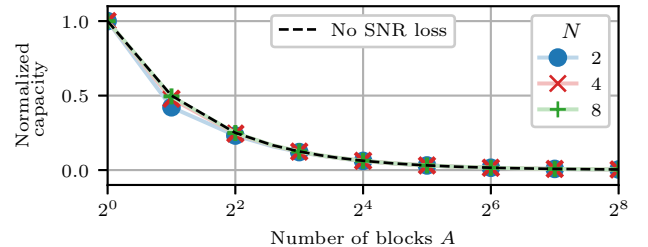


Fig. 11. System communications capacity as a function of number of blocks A for selected N values.

The values are normalized to a system without aliasing. The capacity loss due to SNR is negligible for A and N values greater than 4.

To successfully demodulate the ATMA OFDM, the receiver must revert the phase precoding per block applied at the transmitter (24). The failure to do so would result in erroneous demodulation of $\lfloor A/2 \rfloor$ of the subcarrier blocks. Another problem is the per-block power variations introduced by aliasing. When the per-block power variations are accounted for at the receiver, the subcarrier symbols per block are equalized to match the amplitude of the demodulating (reference) constellation; no degradation in performance should be observed. If the amplitude variations per subcarrier block are unaccounted for in the receiver, then the power variations per subcarrier block will introduce amplitude errors in the demodulation. The error-vector magnitude (EVM) resulting from the amplitude mismatch per subcarrier block can be calculated as

$$\text{EVM} = \sqrt{\frac{1}{A} \sum_{i \in i_{bb}} (\alpha_A(i, d) - 1)^2}. \quad (36)$$

As observed before, the power variation per subcarrier block diminishes with the growing number of blocks and phase shifts. Similarly, the EVM is reduced by increasing A and N as shown in Fig. 12 and Fig. 13.

The key parameters of an ATMA OFDM system are: symbol rate (35), switching frequency (12), phase shifting resolution (13) and ACLR (25). Consider some maximum supported switching frequency $f_{\text{sw max}}$ expressed as a fraction of bandwidth. The minimum aliasing factor is $A_{\text{min}} = B/f_{\text{sw max}}$. Knowing the minimum aliasing factor, the maximum oversampling factor can be calculated as follows $O_{\tau \text{ max}} = A/A_{\text{min}}$. The maximum value of A is not constrained, but increasing

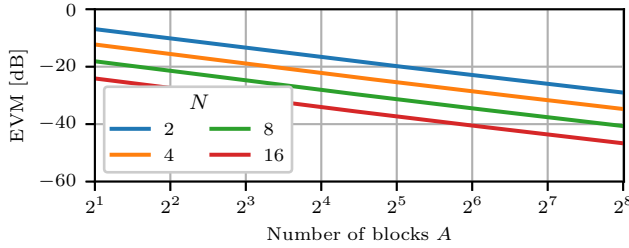


Fig. 12. EVM as a function of number of phase shift values N for selected number of blocks A .

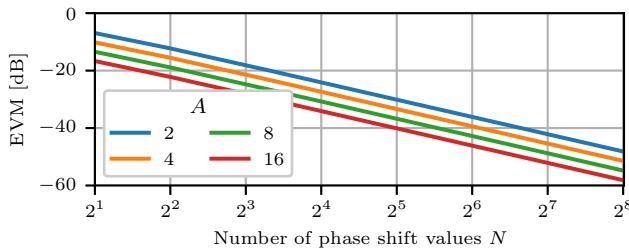


Fig. 13. EVM as a function of number of blocks A for selected number of phase shift values N .

TABLE II
SYSTEM PARAMETERS FOR DIFFERENT ALLOCATIONS OF A AND O_{τ} FOR $N_{\text{cp}} = 0.25K$, $N = 4$ AND $f_{\text{sw max}} = 1/4B$.

Allocation	R [B]	f_{sw} [B]	D	ACLR [dB]
$A = 4, O_{\tau} = 1$	$1/5$	$1/4$	4	19.71
$A = 8, O_{\tau} = 2$	$1/10$	$1/4$	8	22.04
$A = 16, O_{\tau} = 2$	$1/20$	$1/8$	8	24.66
$A = 64, O_{\tau} = 4$	$1/80$	$1/16$	16	30.34

it reduces the symbol rate. For example consider a system of bandwidth B , $N_{\text{cp}} = 0.25K$, $N = 4$ and $f_{\text{sw max}} = 1/4B$. The A and O_{τ} can be allocated in numerous ways. Tab. II presents the system parameters for a few configurations of A and O_{τ} . Increasing A enables higher values of the oversampling at the cost of a significantly reduced communication rate. When considering the ATMA scheme in the context of the antenna array, each antenna is preceded by an identical time modulator front-end module. Therefore, any circuitry losses and imperfections will identically affect all antenna elements and scale linearly with the number of antennas. Due to the reduced communication rate, the system is envisioned to be used in radar-centric joint communications and sensing systems. The repeated block structure does not negatively affect the performance of OFDM radar when the zero-forcing channel estimation is considered.

III. EXPERIMENTAL VALIDATION

The feasibility of the proposed sideband reduction method has been experimentally validated with a one-bit phase shifter. For the experiment, a simple 1-bit phase shifter was constructed using a single-pole double-throw switch ZASWA-2-50DR+ RF switch. The two switch outputs were connected to the combiner directly and via a manual tunable phase shifter. The center frequency of the experimental setup was 2.5 GHz. The phase difference between the two switch-controlled paths was calibrated to 180° . The measured gain mismatch due to different path attenuation was around 0.1 dB and the phase shift difference error was below 1° . The illustration of the experimental setup can be found in Fig. 14. The proposed method is envisioned for multiple antenna systems; however, as each antenna is supposed to be equipped with identical time modulators, it is sufficient to demonstrate the performance of a single module.

The measurement was performed for different numbers of blocks (aliasing factor) and two scenarios. In both scenarios, the center frequency of the transmitted passband signal was

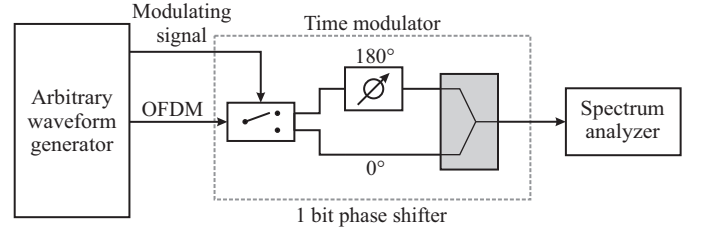


Fig. 14. Illustration of the experimental setup.

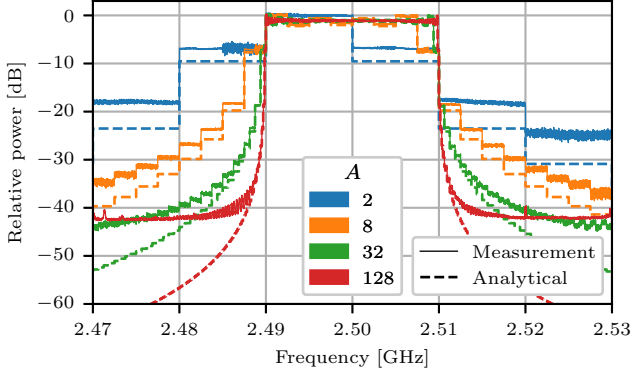


Fig. 15. Measured spectrum of the ATMA for $N = 2$, a constant signal bandwidth $B = 20$ MHz and different number of blocks. The switching frequency is adjusted as $f_{sw} = B/A$.

adjusted to compensate for the frequency offset due to time modulation. This results in spectra always centered at 2.5 GHz for ease of comparison. To guarantee high-resolution spectrum measurement, the number of subcarriers K was 16384. For each measurement, the spectrum is normalized with regard to its maximum. The analytical results are also normalized to the maximum of each trace. In the first scenario, the transmitted signal bandwidth is constant while the switching frequency is adjusted to introduce aliasing for different numbers of blocks $f_{sw} = B/A$. Fig. 15 compares the measured and theoretical values for the first scenario. As expected, increasing the number of blocks efficiently reduces the sideband radiation. In the second scenario, the switching frequency is constant $f_{sw} = 1$ MHz and the signal bandwidth is adjusted with the number of blocks to introduce aliasing $B = Af_{sw}$. This scenario is devised to present the wideband performance of the proposed method. As shown in Fig. 16, the method supports wideband signals.

A discrepancy between the measured and analytical power levels per block can be observed for both scenarios. This can be attributed to the imperfections of the hardware, such as phase and amplitude imbalance between the phase shifter states, leading to imperfect aliasing and the presence of residual power. The amplitude imbalance between the states results in an asymmetrical waveform and introduces a DC component in the harmonics generated by the switching. The limited bandwidth supported by the switch and the non-negligible switching transients introduce tapering of the harmonic powers as their frequency increases. All those effects add up to the total performance degradation and imperfect aliasing of the blocks. Mentioned imperfections scale with the switching frequency and the number of blocks, posing a practical constraint on the number of aliasing blocks.

IV. CONCLUSION

The proposed ATMA architecture allows reducing sideband radiation and switching frequency by splitting the baseband signal into repeated blocks, which are differently precoded and later aliased. The number of blocks is an additional dimension

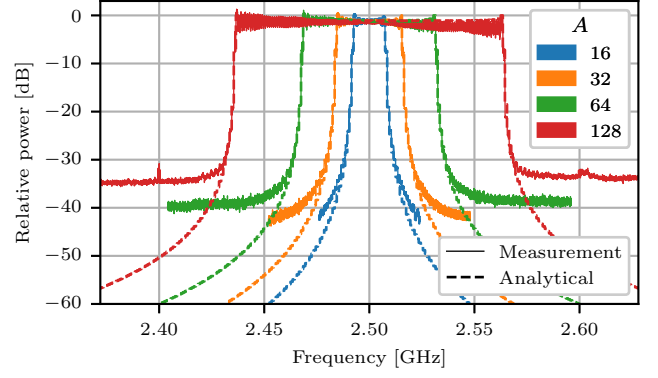


Fig. 16. Measured spectrum of the ATMA for $N = 2$, a constant switching frequency $f_{sw} = 1$ MHz and different number of blocks. The signal bandwidth is adjusted as $B = Af_{sw}$.

that can be tuned along with the phase shifter resolution N to reduce the sideband radiation and allow the TMA to meet the ACLR criteria of a conventional system while having a simpler architecture. The oversampling with aliased TMA requires an additional precoder for each oversampling factor O_τ , limiting the practicality of large oversampling. Since the scheme preserves the total bandwidth but reduces the spectral efficiency, it is well-suited for radar applications as well as radar-centric integrated communication and sensing systems.

REFERENCES

- [1] H. Tataria, M. Shafi, A. F. Molisch, M. Dohler, H. Sjöland, and F. Tufvesson, "6G wireless systems: Vision, requirements, challenges, insights, and opportunities," *Proceedings of the IEEE*, vol. 109, no. 7, pp. 1166–1199, 2021.
- [2] C. Fulton, M. Yeary, D. Thompson, J. Lake, and A. Mitchell, "Digital phased arrays: Challenges and opportunities," *Proceedings of the IEEE*, vol. 104, no. 3, pp. 487–503, 2016.
- [3] A. Valdes-Garcia, B. Sadhu, X. Gu, J.-O. Plouchart, M. Yeck, and D. Friedman, "Scaling millimeter-wave phased arrays: Challenges and solutions," in *2018 IEEE BiCMOS and Compound Semiconductor Integrated Circuits and Technology Symposium (BCICTS)*, 2018, pp. 80–84.
- [4] P. Rocca, G. Oliveri, R. J. Mailloux, and A. Massa, "Unconventional phased array architectures and design methodologies—a review," *Proceedings of the IEEE*, vol. 104, no. 3, pp. 544–560, 2016.
- [5] L. P. P. Rocca, F. Yang and S. Yang, "Time-modulated array antennas – theory, techniques, and applications," *Journal of Electromagnetic Waves and Applications*, vol. 33, no. 12, pp. 1503–1531, 2019.
- [6] H. Shanks, "A new technique for electronic scanning," *IRE Transactions on Antennas and Propagation*, vol. 9, no. 2, pp. 162–166, 1961.
- [7] Q. Zeng, P. Yang, L. Yin, H. Lin, C. Wu, F. Yang, and S. Yang, "Phase modulation technique for harmonic beamforming in time-modulated arrays," *IEEE Transactions on Antennas and Propagation*, vol. 70, no. 3, pp. 1976–1988, 2022.
- [8] A. M. Niknejad and H. Hashemi, *Mm-Wave Silicon Technology: 60 GHz and Beyond*, 1st ed. Springer Publishing Company, Incorporated, 2008.
- [9] F. Ellinger, *Radio Frequency Integrated Circuits and Technologies*. Springer Publishing Company, Incorporated, 01 2007.
- [10] W.-Q. Wang, H. C. So, and A. Farina, "An overview on time/frequency modulated array processing," *IEEE Journal of Selected Topics in Signal Processing*, vol. 11, no. 2, pp. 228–246, 2017.
- [11] M. Wachowiak, A. Bourdoux, and S. Pollin, "Beamforming with over-sampled time-modulated arrays," in *2025 19th European Conference on Antennas and Propagation (EuCAP)*, 2025, pp. 1–5.
- [12] J. C. Bregains, J. Fondevila-Gomez, G. Franceschetti, and F. Ares, "Signal radiation and power losses of time-modulated arrays," *IEEE Transactions on Antennas and Propagation*, vol. 56, no. 6, pp. 1799–1804, 2008.

- [13] L. Poli, P. Rocca, G. Oliveri, and A. Massa, "Harmonic beamforming in time-modulated linear arrays," *IEEE Transactions on Antennas and Propagation*, vol. 59, no. 7, pp. 2538–2545, 2011.
- [14] G. Ni, C. He, Y. Gao, J. Chen, and R. Jin, "High-efficiency modulation and harmonic beam scanning in time-modulated array," *IEEE Transactions on Antennas and Propagation*, vol. 71, no. 1, pp. 368–380, 2023.
- [15] S. Yang, Y. B. Gan, A. Qing, and P. K. Tan, "Design of a uniform amplitude time modulated linear array with optimized time sequences," *IEEE Transactions on Antennas and Propagation*, vol. 53, no. 7, pp. 2337–2339, 2005.
- [16] S. Yang, Y. B. Gan, and A. Qing, "Sideband suppression in time-modulated linear arrays by the differential evolution algorithm," *IEEE Antennas and Wireless Propagation Letters*, vol. 1, pp. 173–175, 2002.
- [17] J. Yang, W. Li, and X. Shi, "Phase modulation technique for four-dimensional arrays," *IEEE Antennas and Wireless Propagation Letters*, vol. 13, pp. 1393–1396, 2014.
- [18] L. Manica, P. Rocca, L. Poli, and A. Massa, "Almost time-independent performance in time-modulated linear arrays," *IEEE Antennas and Wireless Propagation Letters*, vol. 8, pp. 843–846, 2009.
- [19] C. He, H. Yu, X. Liang, J. Geng, and R. Jin, "Sideband radiation level suppression in time-modulated array by nonuniform period modulation," *IEEE Antennas and Wireless Propagation Letters*, vol. 14, pp. 606–609, 2015.
- [20] H. Li, Y. Chen, and S. Yang, "A time-modulated antenna array with continuous sideband spectrum distribution," *IEEE Transactions on Antennas and Propagation*, vol. 71, no. 2, pp. 1557–1567, 2023.
- [21] J. Guo, S. Yang, Y. Chen, P. Rocca, J. Hu, and A. Massa, "Efficient sideband suppression in 4-D antenna arrays through multiple time modulation frequencies," *IEEE Transactions on Antennas and Propagation*, vol. 65, no. 12, pp. 7063–7072, 2017.
- [22] A.-M. Yao, W. Wu, and D.-G. Fang, "Single-sideband time-modulated phased array," *IEEE Transactions on Antennas and Propagation*, vol. 63, no. 5, pp. 1957–1968, 2015.
- [23] Q. Chen, J.-D. Zhang, D.-Y. Luo, W. Wu, Y. Yu, and D.-G. Fang, "Low-sidelobe single-sideband time-modulated phased array using stepped waveforms with different amplitudes," *IEEE Transactions on Antennas and Propagation*, vol. 71, no. 12, pp. 9643–9654, 2023.
- [24] —, "Low-sidelobe single-sideband time-modulated phased array using stepped waveforms with different amplitudes," *IEEE Transactions on Antennas and Propagation*, vol. 71, no. 12, pp. 9643–9654, 2023.
- [25] Q. Chen, J.-D. Zhang, W. Wu, and D.-G. Fang, "A single-sideband time-modulated phased array with low sideband level suitable for wide-bandwidth signals," *IEEE Transactions on Antennas and Propagation*, vol. 70, no. 2, pp. 1057–1067, 2022.
- [26] —, "Enhanced single-sideband time-modulated phased array with lower sideband level and loss," *IEEE Transactions on Antennas and Propagation*, vol. 68, no. 1, pp. 275–286, 2020.
- [27] Y. Gao, G. Ni, K. Wang, Y. Liu, C. He, R. Jin, and X. Liang, "Single-sideband time-modulated phased array with 2-bit phased shifters," in *2020 9th Asia-Pacific Conference on Antennas and Propagation (APCAP)*, 2020, pp. 1–2.
- [28] Y. Gao, X. Liang, J. Chen, J. Chen, and R. Jin, "A high-resolution amplitude-phase control method for 2-bit time-modulated phased arrays," *IEEE Transactions on Antennas and Propagation*, vol. 71, no. 11, pp. 8692–8703, 2023.
- [29] A.-M. Yao, W. Wu, and D.-G. Fang, "Single-sideband time-modulated phased array," *IEEE Transactions on Antennas and Propagation*, vol. 63, no. 5, pp. 1957–1968, 2015.
- [30] ETSI, "5G; NR; Base Station (BS) radio transmission and reception," 3GPP, Tech. Rep. TS 138 104 V16.4.0, 2021.